White Synchrotron Radiation Topography of (1$\bar{1}$0) Nickel Single Crystal

The influence of a [1$\bar{1}$0] Magnetic Field

J. D. Stephenson

Freie Universität Berlin and Fritz-Haber Institut der Max-Planck-Gesellschaft, Berlin

Z. Naturforsch. **37a**, 505—511 (1982); received March 8, 1982

Dedicated to Prof. G. Hildebrandt on the occasion of his 60th birthday

Changes in 70.53° magnetic domain structure on the surface of a perfect (1$\bar{1}$0) nickel crystal have been observed using white synchrotron X-radiation topography. The crystal was influenced by a variable [1$\bar{1}$0] magnetic field. At field strengths $\gtrsim 100$ A/m [11$\bar{1}$]-spike domains, thought to be traces of [011], 70.53° (oblique) magnetic domain walls, appeared within [111]-bands (0.4 mm wide) in the topographs. Reversal of the field produced similar spikes at equivalent field values but in different regions of the crystal.

1. Introduction

Conventional X-ray topography of nickel crystals has been seriously restricted by the lack of perfection in commercially grown crystals, but in several cases individual groups have succeeded in growing almost perfect single crystals of variable size and quality.

De Blois [1] and Chikaura, Fukumori, and Nagakura [2] grew platelike crystals (10 and 50 μm thick, respectively, prepared by chemical reduction of nickel bromide) which the latter authors reported too thin to show good X-ray dynamical contrast of magnetic domain walls. Alex, Tikhonov, and Brümmer [3], using a textured induced secondary recrystallization and strain anneal process, produced thicker (111) nickel crystals from which [$\bar{1}$10], [0$\bar{1}$1] and [10$\bar{1}$] Bloch walls were observed in conventional X-ray (CuKα) 0$\bar{2}$2-topographs. More recently Kuriyama, Boettinger, and Burdette [4] succeeded in growing highly perfect (Czochralski grown) nickel crystal boules, with growth directions along [211], [311] or close to [111], which were eventually sliced into (1$\bar{1}$0) discs (0.4 to 0.6 mm thick) using an acid saw.

11$\bar{1}$-X-ray diffraction (CuKα-transmission) topographs of these specimens by Kuriyama, Boettinger, and Burdette [5], using an asymmetric (double) crystal topographic (ACT) camera (Kuriyama, Early, and Burdette [6], Boettinger, Burdette, Kuriyama, and Green [7]) revealed 70.53° and 109.47° magnetic domain walls whose surface traces were along [110] and [001]. Additional [11$\bar{1}$] alternate darkgrey band structure ≈ 500 μm in width was also observed by Kuriyama, Boettinger and Burdette [8]. Comparison with similar band structure observed in Bragg reflection topographs of the opposite (entrance) crystal surface indicated that the bands were 70.53° domain walls oblique to the surface extending through the entire thickness of the crystal [5].

In other ACT $\bar{1}\bar{1}$1-transmission topographs a line structure of (101) planar defects was observed by Boettinger, Burdette, and Kuriyama [9] which was dark in the direct O-beam and white in the diffracted H-beam [5]. Further, when the crystal was magnetized along a [11$\bar{1}$] (easy magnetization) direction using a rather strong magnetic field of $H = 23900$ A/m, all types of domain contrast disappeared. They reappeared when the field was removed.

The purpose of this paper is to give a preliminary report of alternative domain movement and creation in a perfect nickel crystal in addition to those observations reported in [5, 8, 9]. In this experiment, a relatively small [1$\bar{1}$0] magnetic field (0 to 425 A/m) is applied to the crystal surface. Optimum domain contrast in this case is observed in Laue (back reflection) topographs by rotating the crystal 25° about the [001] horizontal axis towards the white synchrotron radiation (S. R.) beam (HASYLAB, Hamburg).

Reprint requests to Dr. J. D. Stephenson, Fritz-Haber Institut der Max-Planck-Gesellschaft, Faradayweg 4—6, 1 Berlin 33 (Dahlem), BRD.

0340-4811 / 82 / 0500-0505 $ 01.30/0. — Please order a reprint rather than making your own copy.

2. Domain Structure in Nickel

In contrast to the well known domain structure observed in Fe single crystal whiskers or Fe-Si alloy platelets by Bitter pattern, X-ray topography and following methods, those in nickel, prior to [2, 3, 5], were restricted to surface Kerr magneto-optical and Lorentz or scanning electron microscope techniques. The latter results invariably refer to thin Ni-alloy films deposited on a glass or other substrate and exhibit non linear magnetic domain stripe structure associated with epitaxial (mismatch) surface stress. More recent experiments in this field are those of Schroeder and Kronmüller [10] using Kerr magnetooptical and X-ray (Berg-Barrett) topography techniques, Schwellinger [11] using Lorentz microscopy and Kraan and Rekveldt [12] using neutron depolarization in bulk specimens.

As is well reported, nickel differs from iron in that it has a FCC structure with easy magnetization directions along the $\langle 111 \rangle$ cube diagonals, a relatively lower magnetic anisotropy energy density and relatively larger (negative) magnetostriction constants.

The $\langle 111 \rangle$ easy magnetization axes define allowed (minimum energy) directions for the intensity of magnetization vector ($\boldsymbol{M}$) after transversing a domain wall. The remaining two properties imply that magnetic domains in nickel are quite sensitive to small changes in applied external magnetic fields or mechanical stresses.

Nickel domain boundary types have been summarized by Lilley [13] in the form;

Type of boundary		Initial/Final easy directions	
[110],	70.53°	$[\bar{1}1\bar{1}]$,	$[\bar{1}11]$;
[110],	109.47°	$[\bar{1}11]$,	$[1\bar{1}1]$;
[100],	70.53°	$[\bar{1}\bar{1}1]$,	$[\bar{1}\bar{1}\bar{1}]$;
[100],	109.47°	$[\bar{1}\bar{1}1]$,	$[\bar{1}1\bar{1}]$.

In this column each type of wall (70.53° or 109.47°) is preceded by its normal vector which is also the axis of magnetization vector rotation. This definition is used in the following paragraphs to define particular domain walls. Some of the above $\langle 111 \rangle$ values are readjusted to those particular to this experiment.

3. Closure Domain Models

Consider a $(1\bar{1}0)$ nickel crystal with sides (110) and (001) respectively with $\boldsymbol{M}$ initially in the surface and directed along **ab** $[\bar{1}\bar{1}1]$ (Figure 1).

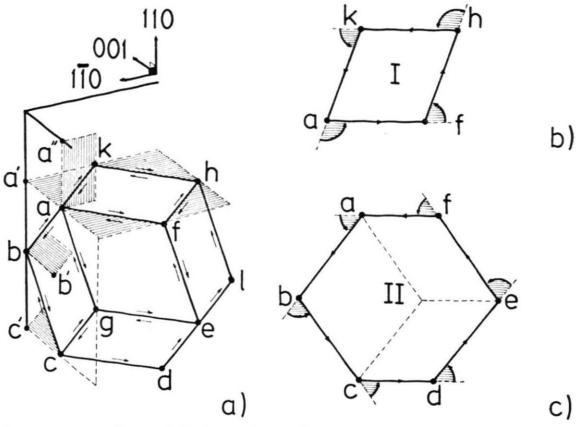

Fig. 1. a) $(1\bar{1}0)$ nickel surface showing the construction of a rhombic duodecahedron of $\langle 111 \rangle$ easy magnetization directions with (shaded) $\langle 100 \rangle$, 70.53° and (arrowed) traces of 180° domain walls. b) Model I; a closed loop of $\langle 111 \rangle$ easy magnetization vectors formed by alternate [110] 70.53° and [110], 109.47° domain walls. The trace of the domain wall lies along [001] in the $(1\bar{1}0)$ surface. c) Model II; a closed loop of $\langle 111 \rangle$ magnetization vectors in nickel formed by successive $\langle 100 \rangle$, 70.53° domain walls **aa′**, **bb′**, **cc′** etc. Magnetization vectors **ab**, **bc** lie in the entrance $(1\bar{1}0)$ surface.

Closed loops of $\langle 111 \rangle$ easy magnetization vectors (see the rhombic duodecahedron, Fig. 1a) can be formed in several ways of which two are described below to show how different types of domain wall may be created;

a) Model I (Fig. 1b) is a (110)-loop, formed by $\langle 111 \rangle$-magnetization vectors which rotate anticlockwise in the (110) plane through 70.53° (at f and k) and 109.47° (at a and h) about [110] normals to the domain wall. This figure was originally given with 180° walls [8] as indicated in Figure 1a.

The rotations may be summarized in the following form;

Model I

Wall type		Position	Initial/Final vectors
[110],	109.47°	a	**ka** $[1\bar{1}\bar{1}]$, **af** $[\bar{1}1\bar{1}]$
[110],	70.53°	f	**af** $[\bar{1}1\bar{1}]$, **fh** $[\bar{1}11]$
[110],	109.47°	h	**fh** $[\bar{1}11]$, **hk** $[1\bar{1}1]$
[110],	70.53°	k	**hk** $[1\bar{1}1]$, **ka** $[1\bar{1}\bar{1}]$

Note that the (110) domain wall, including a, f, h and k, is perpendicular to the $(1\bar{1}0)$ surface which it intersects along [001] (line **aa′** in Fig. 1a) and which is detectable as an [001] domain wall trace

in X-ray topographs. Similar (Model I) faces exist on the rhombic duodecahedron of Fig. 1a which generate other {**110**} closed magnetic loops (and consequent domain walls) oblique to the surface.

Theoretically the [110], 70.53° domain wall is energetically more favourable than [011], 70.53° domain walls.

b) Model II (abcdef, Fig. 1c) is a second type of closed loop involving the rotation of $\boldsymbol{M}$ at ⟨100⟩, 70.53° domain walls which are energetically less favourable than the ⟨110⟩, 70.53° walls of Model I. In this loop $\boldsymbol{M}$ is successively rotated $+\omega - \pi/2$ about ⟨100⟩ on traversing each wall for which we assume an arbitrary rotational energy of say one unit.

The complete (closed) loop abcdefa for Model II can be summarized in the following form;

Model II

Wall Type/Rotation	Position	Initial/Final vectors	Wall energy
$[\bar{1}00]$, $70.53°/\pi/2$	b	**ab** $[\bar{1}\bar{1}1]$, **bc** $[\bar{1}\bar{1}\bar{1}]$	1
$[100]$, $70.53°/\pi/2$	c	**bc** $[\bar{1}\bar{1}\bar{1}]$, **cd** $[\bar{1}1\bar{1}]$	1
$[010]$, $70.53°/\pi/2$	d	**cd** $[\bar{1}1\bar{1}]$, **de** $[11\bar{1}]$	1
$[010]$, $70.53°/\pi/2$	e	**de** $[11\bar{1}]$, **ef** $[111]$	1
$[100]$, $70.53°/\pi/2$	f	**ef** $[111]$, **fa** $[1\bar{1}1]$	1
$[001]$, $70.53°/\pi/2$	a	**fa** $[1\bar{1}1]$, **ab** $[\bar{1}\bar{1}1]$	1

Note that;

i) The closed loop of Model II is non planar; **ab**, **bc** and **df**, ***ef*** are parallel to the $(1\bar{1}0)$ surface and are part of the front (abc) and back (def) of the primitive rhombohedron abcdefga etc.

ii) A combination of two (oblique) $[\bar{1}00]$, 70.53° walls (e.g. at b and c) is rotationally equivalent to a single (oblique) $[\bar{1}00]$, 109.47° wall which requires two units of spin energy for the rotation (see Lilley [13]).

iii) A combination of an (oblique) $[\bar{1}00]$, 109.47° wall with a [010], 70.53° wall (e.g. at b, c and d) is rotationally equivalent to an oblique 180° wall which requires more than two units of rotational energy.

Thus according to the wall energies required in this model, a completely demagnetized nickel crystal, gradually magnetized by an externally applied magnetic field, should show the formation of 70.53° domain walls first, 109.47° domain walls second and (oblique) 180° domain walls last.

This is difficult to realise experimentally due to the spontaneous magnetization and inherent stress in the crystal but the creation and disappearance of oblique [011], or $[10\bar{1}]$, 70.53° domain walls at higher fields is thought to be observable in the form of surface spike domains and described in the next section.

4. Experimental

4.1. Conditions

Initially the crystal (0.6 mm thick, dimension 20×10 mm^2) was arranged with [001] horizontal, [110] vertical and $[1\bar{1}0]$ antiparallel to the S. R. beam. Helmholtz coils were placed on either side of the crystal and coaxial with the beam.

As the electron beam energy in the storage ring at the time of the experiment was 3.3 GeV, the peak intensity of the emitted white spectral distribution was biased towards the longer X-ray wavelength region and (Laue pattern) back reflection topography was therefore employed.

From computer simulated Laue (gnomonic projection) patterns (Stephenson [14]) it was seen that a strong 400-reflection could be obtained by rotating the crystal 25° about the [001] axis (see Figure 2). The operative wavelength forming this topograph is 166 pm ($\lambda/2$ harmonic of the fundamental 200-reflection) which is very close to and on the low absorption side of the nickel K-shell edge ($\lambda_K = 149$ pm).

The resulting Laue pattern (back reflection) topographs, produced on a flat film (Kodak Type R, 100×100 mm^2) mounted perpendicular to the beam, showed good domain contrast in the 400- and to a lesser extent in the accompanying topographs.

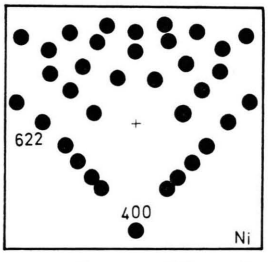

Fig. 2. Computed Laue (back reflection) pattern [14] formed on a flat film (100×100 mm^2) 50 mm distant from the $(1\bar{1}0)$ nickel crystal. The crystal was rotated 25° into the beam about the [001] (horizontal) axis.

4.2. Crystal Perfection

In order to determine a degree of perfection of the nickel crystal used in this experiment, Fig. 3 shows a comparison between two Laue (back reflection) S. R. topographs taken of

i) a $(1\bar{1}0)$ nearly perfect nickel crystal * (400-topograph) and

ii) a (100) commercial crystal (402-topograph).

In both cases a copper wire mesh was placed in front of the crystal and film and normal to the beam, to detect local crystal misorientations — a technique first introduced by Borrmann [15, 16] with calcite crystals. The (projected) image of the mesh is exactly reproduced in the perfect crystal topograph and in very distorted form in that of the (non perfect) commercial crystal.

* Kindly provided by Dr. M. Kuriyama, N.B.S., Washington, U.S.A.

4.3. Domain Movement and Contrast

Figure 4 shows 622-Laue (back reflection) topographs of the $(1\bar{1}0)$ nickel crystal (rotated 25° about [001]) at applied magnetic fields of a) $H_c = 0$ and b) $H_c = 410$ A/m. The topographs are mainly formed by an operative wavelength of 101 pm. 70.53° domain walls are visible along [110] and [001]

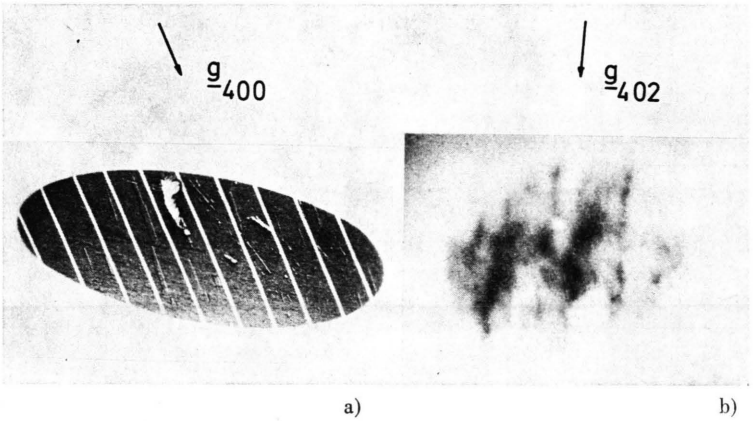

Fig. 3. Synchrotron radiation Laue pattern (back reflection) topographs of a) a nearly perfect single crystal ($\varnothing = 4$ mm, 400-topograph), b) a commercial "single crystal" ($\varnothing = 4$ mm, 402-topograph). A copper wire mesh was placed in front of each crystal during exposure. Its exact (projected) replica appears in the perfect crystal topograph but is completely blurred in that of the non perfect crystal. In a) note (top centre) a small overlap of the white (local distortion) region of the otherwise perfect crystal with the wire image. S.R. conditions 3.3 GeV, 40 mA, 40 s. (Positive prints).

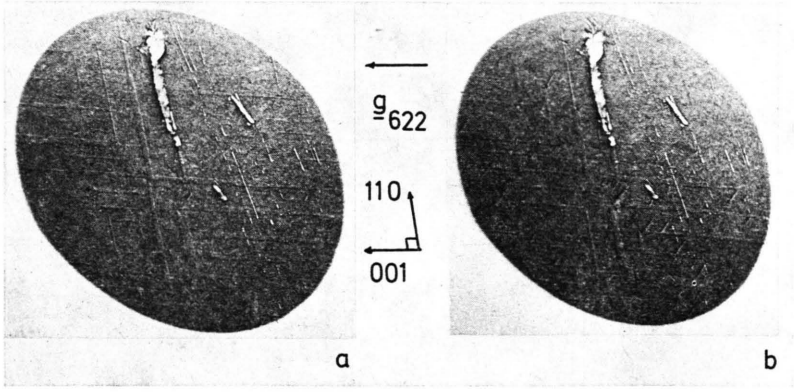

Fig. 4. 622-Laue (back reflection) S.R. topographs of a perfect $(1\bar{1}0)$ nickel crystal, formed by a wavelength 101 pm and subjected to magnetic fields a) $H_c = 0$ A/m, b) $H_c = 410$ A/m. 70.53° domain walls are visible along [110] and [001]; $[11\bar{1}]$-Spike domains appear in b). No zig-zag domain walls are visible. Crystal conditions; 0.6 mm thick, $\varnothing = 4$ mm; S.R. conditions 3.3 GeV, 40 mA, 40 s. (Positive prints).

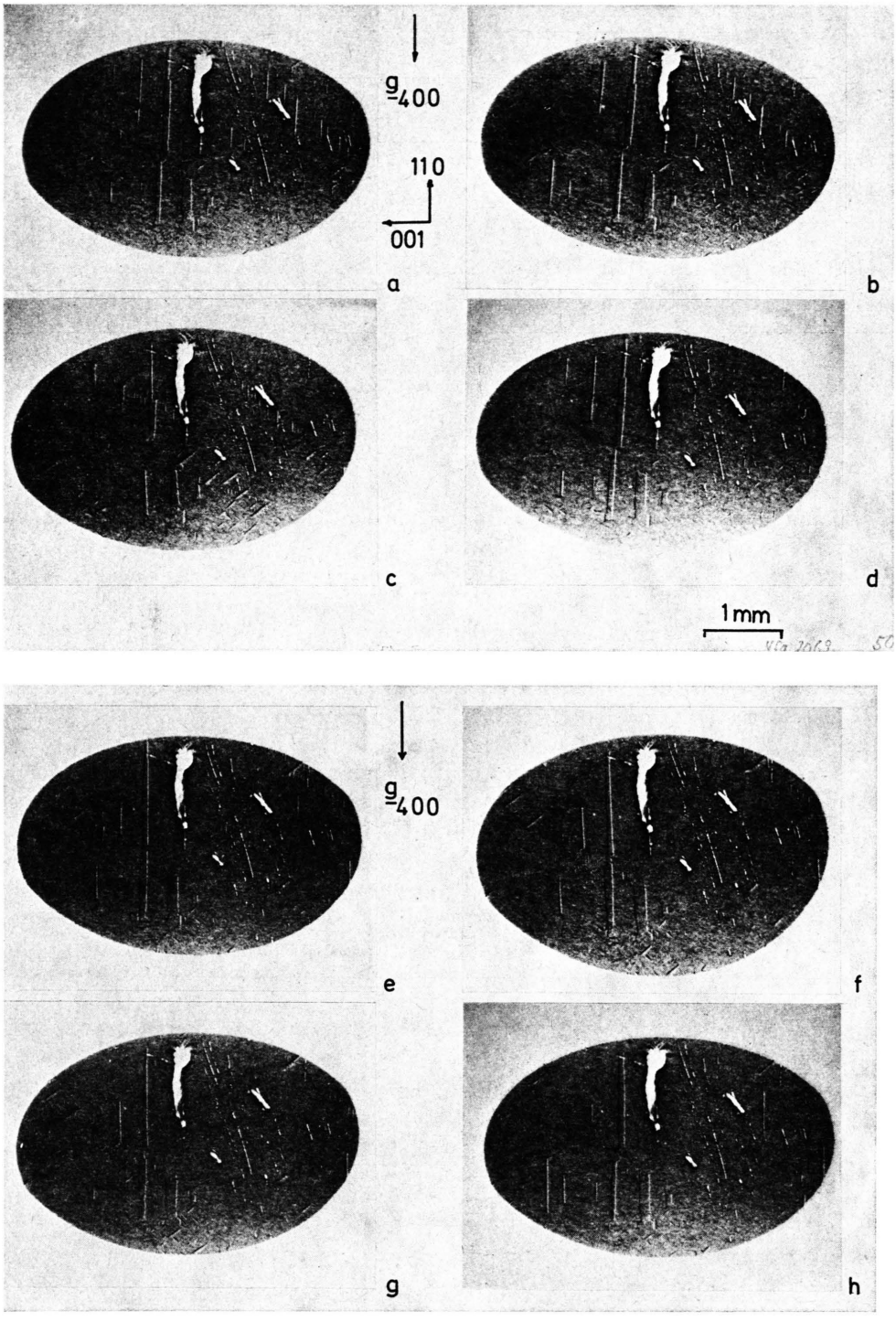

Fig. 5. A series of 400-Laue pattern (back reflection) topographs formed by a wavelength of 166 pm showing the effect of an applied (part hysteresis cycle) magnetic field. a) $H_c = 0$ A/m; b) $H_c = 102$ A/m; c) $H_c = 424$ A/m; d) $H_c = 0$ A/m; e) $H_c = -102$ A/m; f) $H_c = -305$ A/m; g) $H_c = -426$ A/m; h) $H_c = -102$ A/m. Extinction contrast conditions [17] have removed domains along [001]. (Positive prints).

Table 1. Agreement between theoretical and observed topographic contrast conditions occurs for domain walls; a) [110], 70.53° (**aa'**, Fig. 1a) and b) [$\bar{1}$00], 70.53° (**bb'**, Fig. 1a) and [001], 70.53° (**aa''**, Fig. 1a) which are respectively perpendicular, oblique and perpendicular to the (1$\bar{1}$0) surface.

Wall type	M_1	M_2	$\Delta M = M_2 - M_1$	$g_{400} \cdot \Delta M$	Contrast observed?	$g_{622} \cdot \Delta M$	Contrast observed?
Model I							
[110], 109.47°	**ka** [1$\bar{1}\bar{1}$]	**af** [$\bar{1}$1$\bar{1}$]	[$\bar{1}$10]	= 0 contrast	No	= 0 contrast	Yes/No*
[110], 70.53°	**af** [$\bar{1}$1$\bar{1}$]	**fh** [$\bar{1}$11]	[001]	≠ 0 no contrast	Yes	= 0 contrast	Yes
Model II							
[$\bar{1}$00], 70.53°	**ab** [$\bar{1}\bar{1}$1]	**bc** [$\bar{1}\bar{1}\bar{1}$]	[00$\bar{1}$]	≠ 0 no contrast	Yes	= 0 contrast	Yes
[001], 70.53°	**fa** [1$\bar{1}$1]	**ab** [$\bar{1}\bar{1}$1]	[$\bar{1}$00]	= 0 contrast	Yes	= 0 contrast	Yes
[$\bar{1}$00], 109.47°	**ab** [$\bar{1}\bar{1}$1]	**ch** [$\bar{1}$1$\bar{1}$]	[01$\bar{1}$]	≠ 0 no contrast	Yes	≠ 0 no contrast	No

* Indecisive — the observed contrast could also be due to the [110], 70.53° wall.

which contract in width and length at the higher field and in some cases disappear. [11$\bar{1}$]-spike (domains) are clearly visible in Figure 1b.

The film was placed 50 mm in front of the crystal with S. R. conditions 3 GeV, 40 mA; film exposure time 40 s.

Figure 5 shows a more complete series of 400-topographs recorded at different settings of the applied (hysteresis cycle) field. The topographs are mainly formed by an X-ray wavelength of 166 pm; S. R. conditions as in Figure 4. Notice the absence of the "horizontal" domains directed along [001] possibly due to extinction contrast conditions (Polcarová and Kaczér [17]) which in this case are

$$\boldsymbol{g}_{400} \cdot (\boldsymbol{M}_2 - \boldsymbol{M}_1) = 0 \quad \text{(no contrast)} \qquad (1\,\text{a})$$

and

$$\boldsymbol{g}_{400} \cdot (\boldsymbol{M}_2 - \boldsymbol{M}_1) \neq 0 \quad \text{(contrast)}, \qquad (1\,\text{b})$$

$\boldsymbol{M}_1$ and $\boldsymbol{M}_2$ being the magnetization vectors either side of the domain wall (see appendix).

A preliminary analysis of the contrast observed in the 400- and 622-topographs, using models I and II, Fig. 1, is given in Table 1 from which it appears that the observed domain walls are [110], 70.53° (**aa'**), [$\bar{1}$00], 70.53° (**bb'**) and [001], 70.53° (**aa''**) which are respectively perpendicular, oblique and perpendicular to (1$\bar{1}$0).

In the series of 400-topographs, shown in Fig. 5, [11$\bar{1}$]-spikes (≈0.4 mm long) and smaller [$\bar{1}\bar{1}$0]-spikes begin to grow from the inherent domain walls at relatively small applied fields (see also Figure 4). They appear to be formed mainly within [111] surface bands (width ≈0.4 mm, spaced ≈0.8 mm apart). The spikes disappear when the field is returned to zero.

The [11$\bar{1}$]-spikes are consistent with magnetic domain surface traces associated with (oblique) [011], or [0$\bar{1}\bar{1}$], 70.53° domain walls. Oblique 70.53° domain walls were also observed by Kuriyama et al. [9] in similar nickel crystals. In the latter case they appeared as dark-grey [11$\bar{1}$] bands which extended completely through the crystal.

Reversal of the field produces the reverse effects, i.e. extension and broadening of the [110], 70.53° [$\bar{1}$00], 70.53° and [001], 70.53° domain areas. [11$\bar{1}$]-spike domains reappear at the maximum reverse field ($H_c = -425$ A/m) again within surface bands

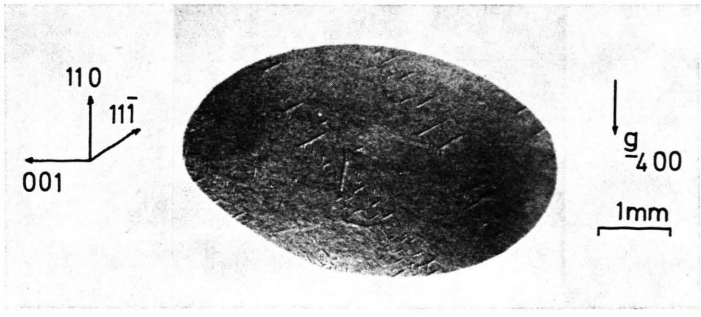

Fig. 6. 400-topograph of another part of the crystal showing spike formation along [11$\bar{1}$] at higher magnetic fields (H_c = 426 A/m). (Positive print).

directed along [111] but between those obtained with positive fields (cf. Figs. 5c and 5g).

A clearer picture of the band arrangement of the [11$\bar{1}$]-spike growth at $H_c = 420$ A/m in another part of the crystal is shown in the 400-topograph of Figure 6.

It appears that the application of the magnetic field produces a sandwich type distribution of stress in the crystal. From magnetostriction considerations (large negative magnetostriction constants for nickel) the creation of [11$\bar{1}$]-spikes within [111] bands implies a [11$\bar{1}$] (component) tensile stress in these regions.

In this respect, an earlier report by Kuriyama et al. [5] indicated that of the many possible 180° domains theoretically present on the (1$\bar{1}$0) surface (see Fig. 1a), contrast may be possible from 180° domain walls oblique to the surface — it was assumed in this case that a significant local strain distribution existed near the wall-surface intersection. 180° domain walls perpendicular to the surface are well known to give no contrast under all diffraction conditions.

Acknowledgements

The research was supported by the Bundesministerium für Forschung und Technologie. Thanks are given to Prof. C. Kunz and members of the Deutsches Elektronen Synchroton, Hamburg, for permission to use the DORIS facility, Prof. G. Hildebrandt for kindly reading through the script and helpful discussions and last but not least to Dr. M. Kuriyama, National Bureau of Standards, Washington, USA, for the gracious loan of a nickel crystal and comments.

Note added in proof

Dr. Kuriyama Comments; The visibility and invisibility (domain) conditions are most likely more complex than the well known $g \cdot \Delta M$ rule given in Eqs. (1a) and (1b) of this paper (see]9]).

[1] R. W. De Blois, J. A. P., **36**, 1647 (1965).
[2] Y. Chikaura, H. Fukumori, and S. Nagakura, Jap. J. Appl. Phys., **11**, 1582 (1972).
[3] V. Alex, L. V. Tikhonov, and O. Brümmer, Kristall u. Technik **9**, 643 (1974).
[4] M. Kuriyama, W. J. Boettinger, and H. E. Burdette, Nat. Bureau of Standards, Publ. N° NBS IR 76—980, (1976), unpublished; J. Cryst. Growth. **43**, 287 (1978).
[5] M. Kuriyama, W. J. Boettinger, and H. E. Burdette, J. Appl. Phys. **47**, 5064 (1977): J. Mat. Sci. **12**, 353 (1977).
[6] M. Kuriyama, J. G. Early, and H. E. Burdette, J. Appl. Cryst. **7**, 535 (1974).
[7] W. J. Boettinger, H. E. Burdette, M. Kuriyama, and R. E. Green, Rev. Sci. Instrum. **47**, 906 (1976).
[8] M. Kuriyama, W. J. Boettinger, and H. E. Burdette, Adv. in X-ray Analysis, **20**, 245 (1977).
[9] W. J. Boettinger, H. E. Burdette, and M. Kuriyama, Phil. Mag. **36**, 763 (1977).
[10] G. Schroeder and H. Kronmüller, phys. stat. sol. (a) **34**, 623 (1976).
[11] P. Schwellinger, phys. stat. sol. (a) **36**, 335 (1976).
[12] W. H. Kraan and M. Th. Rekveldt, Physics **86—88B**, 1341 (1977).
[13] B. A. Lilley, Phil. Mag. (vii) **41**, 792 (1950).
[14] J. D. Stephenson, phys. stat. sol. (a), **65**, 601 (1981).
[15] G. Borrmann, Optik **10**, 405 (1953).
[16] M. v. Laue, Röntgenstrahl-Interferenzen, Fig. 165 (p. 427). Akad. Verlags-Gesellschaft-Frankfurt (Main) 1960.
[17] M. Polcarová and J. Kaczér, phys. stat. sol. (a) **21**, 653 (1967).